Desalination and Water Treatment
www.deswater.com
doi: 10.1080/19443994.2013.770192

51 (2013) 5942–5953
September

Taylor & Francis
Taylor & Francis Group

Modeling and computer simulation of a reverse osmosis desalination plant—case study of Bousfer plant—Algeria

Belkacem Absar[a,*], Omar Belhamiti[b]

[a]*Laboratoire d'Energie-Environnement et Développement Durable, Université de Mostaganem, 27000 Mostaganem, Algérie*
Tel. +213 55 51 14 360; Fax: +213 45 33 13 38; email: abbelkacem@univ-mosta.dz
[b]*Laboratoire de Mathématiques Pures et Appliquées, Université de Mostaganem, 27000 Mostaganem, Algérie*

Received 16 May 2012; Accepted 3 January 2013

ABSTRACT

This work aims to verify the effects of the retentate and the permeate flow pattern and the concentration polarization phenomenon on the performances of a reverse osmosis desalination plant. The two types of flow circulation studied in this work are the co-current and counter-current flow patterns. Two mathematical models were developed. They are both based on the solution diffusion model. The first mathematical model is formed of a set of non-linear equations. The second one is formed of a set of ordinary differential equations. The numerical resolution of the second mathematical model is subjected to the split boundary value problem. A robust and efficient iterative procedure was developed to solve this problem. It consists in combining the orthogonal collocation and the finite elements method. The non-linear coupled system of differential equations is transformed to an uncoupled linear system by an iterative technique. This linearization allows more stability. The real case of reverse osmosis desalination plant of Bousfer, in the west of Algeria, is used to verify the accuracy of the developed mathematical models. The results obtained by simulations show a good adequacy between the experimental values and those obtained by the numerical resolution of the developed models.

Keywords: Bousfer plant; Reverse osmosis; Computer simulation; Flow pattern; Orthogonal collocation; Finite elements method

1. Introduction

The fast growth on the drinking water demand and the irregular rainfall that Algeria knew in the last years leads to the adoption of a new water policy. The use of sea water desalination techniques has become a strategic alternative to ensure drinking water supply for cities of the littoral and others agglomerations. A program of installation of sea water desalination units was made and quickly implemented. Thus, 13 stations of high production capacity from 50,000 up to 500,000 m^3/d and more than 17 monobloc units were built through the Algerian littoral. Most of these units use the reverse osmosis technique.

The reverse osmosis process consists in passing aqueous solution under pressure through an appropriate membrane and withdrawing the membrane permeate at atmospheric pressure and ambient temperature. The product obtained is enriched in pure

*Corresponding author.

1944-3994/1944-3986 © 2013 Balaban Desalination Publications. All rights reserved.

water with a total salinity less than 500 mg/l. The dissolved salts are recovered in the retentate with higher concentration in the high-pressure side of the membrane. The retentate is rejected with a salt concentration ranging from 60 to 70 g/l. For this, the discharge shall be far from the coast to decrease the salt concentration.

A detailed model that describes a general membrane separation process was developed from mass, energy, and momentum balances [1]. This approach disregards some common assumptions and is applicable to any membrane separation. This model was used to assess the performances of a gas separation system in hollow fiber modules.

The structural information, such as the pore size and the skin thickness of the active layer, was used to predict the performances of the reverse osmosis hollow fiber membranes [2]. This study shows that the membrane structure is of primary importance in addition to process design.

Another model based on a generalized transport equation system involving water solvent and ionized solutes was developed [3]. This model was tested to predict the performances of two types of membrane without specifying their configurations.

Wiley and Fletcher [4] utilize computational fluid dynamics to simultaneously model flow and concentration polarization in both feed and permeate channels for pressure-driven membrane processes. The effect of rejection, wall permeation rates, and solutions properties are studied.

A mathematical model based in conservation equation of mass and momentum was developed to determine the factors that affect the performances of pressure-driven membrane processes [5]. This model is used to study the effect of buoyancy in reverse osmosis water desalination. In this work, neither configuration of membrane module (hollow fiber or spiral wound), nor flow pattern is specified.

An optimization algorithm is used to find the optimal design of a reverse osmosis network for sea water desalination [6]. The networks were designed by using hollow fiber module. In this study, only co-current is considered.

Absar et al. [7] developed a mathematical model for a reverse osmosis module operating in closed-loop concentrating mode. Two flow patterns were studied: the co-current and the counter-current. In this mathematical model, the concentration polarization phenomenon was neglected. In our study, two mathematical models are developed. They are both based on the solution-diffusion model. It permits to study the effects of the permeate and the retentate circulation inside the module and the concentration polarization phenomenon on the desalination modules performances.

This work is organized as follows:

- Section 2 gives the fundamental equations that describe the transport phenomena in reverse osmosis using the solution-diffusion model and the material balance equations for the modes of flow rate circulation.
- Section 3 presents the resolution method used to resolve the mathematical model described earlier with a brief review of the orthogonal collocation on the finite elements method.

In sections 4 and 5, mathematical models developed in the previous section are used to simulate the sea water desalination plant of Bousfer, Algeria.

2. Mathematical modeling

The mass transfer model employed in this study is the solution-diffusion model. The solvent mass flux can be expressed by Fick's law. It depends on transmembrane pressure ΔP and the osmotic pressure of the solution on the feed and the permeate side of the membrane [8,9]:

$$J_w = A_w(\Delta P - \Delta\pi) \tag{1}$$

A_w is the water permeability constant.

$\Delta\pi$ is the osmotic pressure difference on both sides of the membrane. Its expression is given as follows:

$$\Delta\pi = \pi_M - \pi_P \tag{2}$$

where the subscripts M refers to the membrane and the subscript P to the permeate side.

For low concentration, the osmotic pressure is approximately a linear function of solute concentrations [10,11]:

$$\pi = \kappa C \tag{3}$$

where κ is a proportionality coefficient [10–12]. By substituting Eq. (3) into Eq. (1), we obtain the following:

$$J_w = A_w(\Delta P - \kappa\Delta C) \tag{4}$$

ΔC is the gradient of the solute concentration. It is expressed as follows:

$$\Delta C = C_M - C_P \tag{5}$$

For the solute flux, it is assumed that chemical potential difference due to pressure is negligible and

so the driving force is almost entirely due to concentration differences.

From Fick's law, the solute mass flux is represented as follows:

$$J_s = B_s(\Delta C) \tag{6}$$

where B_s is the solute permeability coefficient which is a function of the solute composition and the membrane structure.

The solute mass flow rate is expressed as:

$$\dot{Q}_s = J_s S_a = B_s S_a (C_M - C_P) \tag{7}$$

S_a is the membrane surface exchange.

In pressure-driven liquid-phase membrane processes, the solvent as well as the dissolved matters move by convection to the surface of the membrane. The retention of the rejected species on the surface of the membrane forms a polarization layer. Thus, a concentration gradient is formed between the feed solution and the membrane surface.

This phenomenon causes an increase in the solute permeation driving force $(C_M - C_p)$ and a reduction in that of the solvent permeation [11].

The resolution of the solute mass balance equation at the membrane surface gives:

$$\frac{(C_M - C_P)}{(C_F - C_P)} = \exp\left(\frac{J_{vw}}{K}\right) \tag{8}$$

C_P is the salt concentration in the feed side.

J_{vw} is the volumetric flow rate.

C_M is the solute concentration at the membrane surface.

K is the mass transfer coefficient. It depends on the solution physical and chemical properties and also on the system hydrodynamic conditions. Analogies between mass and heat transfer allow calculation of the mass transfer coefficient [13–18].

The membrane rejection is defined as the fraction of solute present in the solution which is stopped by the membrane:

$$T_R = \frac{(C_F - C_P)}{C_F} = 1 - \frac{C_P}{C_F} \tag{9}$$

Using the relations for solvent and solute flux, solute rejection for the solution-diffusion model can be expressed as follows:

$$\frac{1}{T_R} = 1 + \frac{B_s \rho_w}{A_w}\left(\frac{1}{\Delta P - \Delta\pi}\right) \tag{10}$$

Eq. (10) shows that if the pressure tends to a large value, the rejection approaches toward unity.

2.1. First mathematical model

This mathematical model is simple. Its resolution is simple and does not present a particular difficulty. It permits calculation of permeate flow (solvent and solute) knowing certain parameters: solvent and solute properties, salinity, surface exchange, and hydraulic transmembrane pressure.

By substituting ΔC by its expression Eq. (4) in Eq. (5), we obtain:

$$J_w = A_w(\Delta P - \kappa(C_M - C_P)) \tag{11}$$

The solvent flow rate expression can be obtained by multiplying the mass flux expression by the membrane surface and dividing by the density:

$$Q_w = \frac{J_w S_a}{\rho_w} \tag{12}$$

ρ_w is the water density.

$$Q_w = \frac{A_w}{\rho_w} S_a(\Delta P - \kappa(C_M - C_P)) \tag{13}$$

The concentration difference $(C_M - C_p)$ is expressed as follows:

$$(C_M - C_P) = (C_F - C_P)\exp\left(\frac{J_{vw}}{K}\right) \tag{14}$$

C_F is known. It represents the solute concentration in the feed solution.

The solvent volumetric flux, J_{vw} is a function of the volumetric flow rate (Q_w), and the membrane surface (S_a):

$$J_{vw} == \frac{Q_w}{S_a} \tag{15}$$

C_P is the solute concentration in the permeate side. It can be expressed by the ratio of the solute mass flow rate on the solvent volumetric flow rate:

$$C_P = \frac{\dot{Q}_s}{Q_w} \tag{16}$$

By replacing C_p by its expression in Eq. (13):

$$Q_w = \frac{A_w}{\rho_w} S_a\left(\Delta P - \kappa\left(C_F - \frac{\dot{Q}_s}{Q_w}\right)\exp\left(\frac{Q_w}{KS_a}\right)\right) \tag{17}$$

In the same way, we rewrite the solute mass flow rate:

$$Q_s = B_s S_a \kappa \left(C_F - \frac{\dot{Q}_s}{Q_w} \right) \exp\left(\frac{Q_w}{K S_a} \right) \tag{18}$$

The total solvent volumetric flow rate is obtained as follows:

$$Q_p = \frac{Q_w \rho_w + \dot{Q}_s}{\rho_w} \tag{19}$$

Global mass balance equation gives:

$$Q_B = Q_F - Q_P \tag{20}$$

Q_B: retentate volumetric flow rate.
Q_F: feed volumetric flow rate.

Another parameter, which must be taken into consideration in addition to these two equations, is the pressure drop in the feed side PB and the permeate side PP. For the spiral modules, the flow in the feed and permeate side is regarded as a flow between two plates of t spacing, L length and W width. The feed side pressure drop equation is given as follows [9]:

$$\Delta P_B = \frac{12 Q_B L \mu}{W t^3} \tag{21}$$

where μ is the water dynamic viscosity.

The flow in hollow fiber module is similar to an annular flow (two concentric tubes of diameters D_i and D_o). The pressure drop equation is given as follows [19]:

$$\Delta P_B = \frac{128 Q_B L \mu}{\pi (D_o^2 - D_i^2) \left(D_o^2 + D_i^2 - \frac{(D_o^2 - D_i^2)}{\ln\left(\frac{D_o}{D_i}\right)} \right)} \tag{22}$$

The permeate side pressure drop is expressed as follows:

$$\Delta P_P = \frac{8 Q_P L \mu}{\pi r_i^4} \tag{23}$$

This equation is the same for both types of flow pattern.

In the case of the spiral wound module, r_i is the collector radius. For hollow fiber module, r_i is that of fibers.

2.2. Second mathematical model

Co-current and counter-current flow pattern can be met in both configurations: hollow fibers and spiral wounds. Indeed, in both configurations, transfer phenomena are governed by the same laws: solution diffusion model. The flow through a spiral wounds is assumed as a flow though a rectangular channel. On the other hand, the flow through a hollow fiber module can considered as a flow through a tube.

The second mathematical model takes account of the feed and permeate flow rate direction.

2.2.1. Co-current flow pattern

In this flow pattern, permeate and feed in fiber side and shell, respectively, flow co-currently. According to the solution-diffusion model, the rate of water permeate, Q_{pw}, in an elemental section ΔS_a is:

$$Q_w = \frac{A_w}{\rho_w} \Delta S_a \left(\Delta P - \kappa (C_F - C_P) \exp\left(\frac{Q_{pw}}{K \Delta S_a} \right) \right) \tag{24}$$

For hollow fibers configuration, elemental section is expressed as follows:

$$\Delta S_a = \pi D_m \Delta x \tag{25}$$

where D_m is the mean diameter.

$$Q_w = \frac{A_w}{\rho_w} (\pi D_m \Delta x) \left(\Delta P - \kappa (C_F - C_P) \exp\left(\frac{Q_{pw}}{K \Delta S_a} \right) \right) \tag{26}$$

The material balance for water in the shell side is obtained:

$$Q_{sw} = \left(Q_{sw} + \frac{dQ_{sw}}{dx} \Delta x \right) + Q_{pw} \tag{27}$$

where Q_{sw} is the water volumetric flow rate in the shell side, see Figure 1. The first subscript indicates the shell or the fiber side, and the second subscript indicates the solute or the water.This equation reduces to:

$$\frac{dQ_{sw}}{dx} = -\frac{Q_{pw}}{\Delta x} \tag{28}$$

Q_{pw} is the permeate flow rate across the membrane.

Substituting for in Eq. (26):

$$\frac{dQ_{sw}}{dx} = -\frac{A_w}{\rho_w} (\pi D_m) \left(\Delta P - \kappa (C_F - C_P) \exp\left(\frac{Q_{pw}}{K \Delta S_a} \right) \right) \tag{29}$$

C_F indicates the solute concentration in the feed flow rate (shell side). It is expressed as the ratio of the

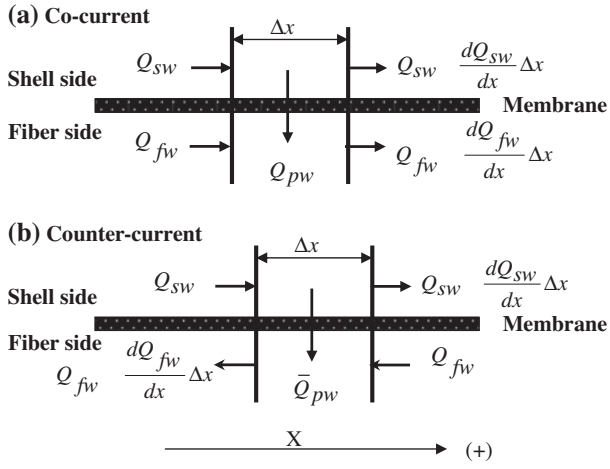

Fig. 1. Flow rate change across △.

solute mass flow rate on the water volumetric flow rate:

$$C_F = \frac{\dot{Q}_{ss}}{Q_{sw}} \tag{30}$$

$\dot{Q}_{ss}$: Solute mass flow rate in the shell side.

Similar equation is obtained for the solute concentration C_P in the permeate flow rate (fiber side):

$$C_p = \frac{\dot{Q}_{fs}}{Q_{fw}} \tag{31}$$

where $\dot{Q}_{fs}$ and Q_{fw} are, respectively, the solute mass flow rate and the water volumetric flow rate in the fiber side.

Substituting C_F and C_p by their expressions in Eq. (29):

$$\frac{dQ_{sw}}{dx} = -\frac{A_w}{\rho_w}(\pi D_m) \times \left(\Delta P - \kappa\left(\frac{\dot{Q}_{ss}}{Q_{sw}} - \frac{\dot{Q}_{fs}}{Q_{fw}}\right)\exp\left(\frac{Q_{pw}}{K\Delta S_a}\right)\right) \tag{32}$$

The material balance for water on the fiber side is obtained in the same manner:

$$\frac{dQ_{fw}}{dx} = \frac{A_w}{\rho_w}(\pi D_m) \times \left(\Delta P - \kappa\left(\frac{\dot{Q}_{ss}}{Q_{sw}} - \frac{\dot{Q}_{fs}}{Q_{fw}}\right)\exp\left(\frac{Q_{pw}}{K\Delta S_a}\right)\right) \tag{33}$$

The material balance for the solute in the shell side is obtained (see Fig. 1):

$$\dot{Q}_{ss} = \left(\dot{Q}_{ss} + \frac{d\dot{Q}_{ss}}{dx}\Delta x\right) + \dot{Q}_{ps} \tag{34}$$

where $\dot{Q}_{ss}$ is the solute mass flow rate in the shell side and $\dot{Q}_{ps}$ the solute mass flow rate across the membrane.

Arranging this equation and substituting $\dot{Q}_{ps}$ by its expression Eq. (7):

$$\frac{d\dot{Q}_{ss}}{dx} = -B_s(\pi D_m)\left(\frac{\dot{Q}_{ss}}{Q_{sw}} - \frac{\dot{Q}_{fs}}{Q_{fw}}\right)\exp\left(\frac{Q_{pw}}{K\Delta S_a}\right) \tag{35}$$

A similar equation is obtained for the fiber side:

$$\frac{d\dot{Q}_{fs}}{dx} = B_s(\pi D_m)\left(\frac{\dot{Q}_{ss}}{Q_{sw}} - \frac{\dot{Q}_{fs}}{Q_{fw}}\right)\exp\left(\frac{Q_{pw}}{K\Delta S_a}\right) \tag{36}$$

Finally, the mathematical model obtained is composed of a set of four ordinary differential equations. To determine the permeate flow rate at the end of the module, the Eqs. (32), (33), (35), and (36) must be integrated simultaneously.

$$\begin{cases} \frac{dQ_{sw}}{dx} = -\frac{A_w}{\rho_w}(\pi D_m)\left(\Delta P - \kappa\left(\frac{\dot{Q}_{ss}}{Q_{sw}} - \frac{\dot{Q}_{fs}}{Q_{fw}}\right)\exp\left(\frac{Q_{pw}}{K\Delta S_a}\right)\right) \\ \frac{dQ_{fw}}{dx} = \frac{A_w}{\rho_w}(\pi D_m)\left(\Delta P - \kappa\left(\frac{\dot{Q}_{ss}}{Q_{sw}} - \frac{\dot{Q}_{fs}}{Q_{fw}}\right)\exp\left(\frac{Q_{pw}}{K\Delta S_a}\right)\right) \\ \frac{d\dot{Q}_{ss}}{dx} = -B_s(\pi D_m)\left(\frac{\dot{Q}_{ss}}{Q_{sw}} - \frac{\dot{Q}_{fs}}{Q_{fw}}\right)\exp\left(\frac{Q_{pw}}{K\Delta S_a}\right) \\ \frac{d\dot{Q}_{fs}}{dx} = B_s(\pi D_m)_s\left(\frac{\dot{Q}_{ss}}{Q_{sw}} - \frac{\dot{Q}_{fs}}{Q_{fw}}\right)\exp\left(\frac{Q_{pw}}{K\Delta S_a}\right) \end{cases} \tag{37}$$

2.2.2. Counter-current flow pattern

In this flow pattern, permeate and feed in fiber and shell side, respectively, flow counter currently. Proceeding in the same manner to that of the co-current flow, we obtain similar equations:

$$\begin{cases} \frac{dQ_{sw}}{dx} = -\frac{A_w}{\rho_w}(\pi D_m)\left(\Delta P - \kappa\left(\frac{\dot{Q}_{ss}}{Q_{sw}} - \frac{\dot{Q}_{fs}}{Q_{fw}}\right)\exp\left(\frac{Q_{pw}}{K\Delta S_a}\right)\right) \\ \frac{dQ_{fw}}{dx} = -\frac{A_w}{\rho_w}(\pi D_m)\left(\Delta P - \kappa\left(\frac{\dot{Q}_{ss}}{Q_{sw}} - \frac{\dot{Q}_{fs}}{Q_{fw}}\right)\exp\left(\frac{Q_{pw}}{K\Delta S_a}\right)\right) \\ \frac{d\dot{Q}_{ss}}{dx} = -B_s(\pi D_m)\left(\frac{\dot{Q}_{ss}}{Q_{sw}} - \frac{\dot{Q}_{fs}}{Q_{fw}}\right)\exp\left(\frac{Q_{pw}}{K\Delta S_a}\right) \\ \frac{d\dot{Q}_{fs}}{dx} = -B_s(\pi D_m)_s\left(\frac{\dot{Q}_{ss}}{Q_{sw}} - \frac{\dot{Q}_{fs}}{Q_{fw}}\right)\exp\left(\frac{Q_{pw}}{K\Delta S_a}\right) \end{cases} \tag{38}$$

These equations constitute the mathematical model for a counter-current flow pattern.

2.3. Proportionality coefficient calculation

For low- and medium-concentration solutions, osmotic pressure is expressed as linear relationship with concentration (Eq. (3)). The proportionality coefficient is calculated as follows [20]:

$$\kappa = \frac{nRT}{M} \tag{39}$$

n is the number of particles. For sea water, majority salt is NaCl ($n = 2$).

M is the molar mass of NaCl ($M = 58.5\,\mathrm{g/mol}$).

R is the gas constant.

$\kappa = 1.097755 \times 10^{+12}\,\mathrm{m^2/h^2}$

2.4. Solvent permeability constant calculation

Solvent (water) permeability is deduced from the solution-diffusion theory. It depends on the membrane characteristics (type and thickness). Presence of salt has no effect [21].

Water permeability constant expression is given as follows:

$$A_w = \frac{D_w C_w v_w}{lRT} \tag{40}$$

D_w: solvent diffusion coefficient.

C_w: solvent mean concentration in membrane.

v_w: solvent partial molar volume.

l: membrane thickness.

R: gas constante.

T: temperature.

Liquids diffusion coefficient is given by De Stokes–Einstein formula [22,23]:

$$D_w = \frac{kT}{6a\mu} \tag{41}$$

k: Boltzmann constant

a is water molecular radius, $a = 1.35$ A [24].

μ is the solution dynamic viscosity. It depends on salinity and temperature. For a salinity of 39 g/l and a temperature of 25°C, dynamic viscosity is 0.9×10^{-3} kg/m s [25].

We obtain a water permeability constant of 4.43882×10^{-13} h/m.

Actual membranes have solvent (water) permeability constant of between 4.16×10^{-13} and 9.72×10^{-13} h/m [23,26].

2.5. Solute permeability constant calculation

This value is given by manufacturer. It can be, however, calculated from Eq. (10), by using the solute rejection value which is a characteristic of the membrane:

$$B_s = \frac{A_w(\Delta P - \Delta\pi)(1 - T_R)}{\rho_w T_R} \tag{42}$$

For a membrane with a rejection salt of 99.5%, solute permeability constant is equal to 1.188896×10^{-4} m/h.

For aromatic polyamide membranes, solute permeability constant is about 1.08×10^{-4} m/h [17].

3. Methods of resolution

The numerical resolution was achieved by the orthogonal collocation on the finite elements methods [7]. This method is used to resolve the split boundary value problem. This choice is justified by the accuracy and the stability if this technique.

The method of orthogonal collocation as described by Villadsen and Michelsen [27] can lead to the numerical resolution of many problems. However, it does not prove very effective for certain cases where the solution is very irregular. To avoid this problem, it is necessary to take a very great order of approximation. It is a disadvantage which limits the application fields of this technique. This is the reason why the orthogonal collocation method is combined with the finite element method.

In this work, the orthogonal collocation on the finite element method as a numerical method to solve the boundary value problems is chosen due to its efficiency and robustness.

Tessendorf et al. [28] have used the orthogonal collocation on finite element method to solve a set of non-linear coupled differential equations. Gauss method was used to solve the non-linear algebraic equations system.

In our approach [7], an iterative technique was developed to uncouple and linearize the system of the differential equations. The non-linear coupled system is thus transformed to an uncoupled linear system. This linearization allows more stability. The numerical resolution of the proposed mathematical model using this procedure has led to results with high precision (check of material balance with high precision).

Our technique consists in giving an initial profile of solution for each equation which verifies the boundary conditions $y_1^{(1)}, y_2^{(2)}, y_3^{(3)}, y_4^{(4)}$.

The iterative procedure can be written as follows:

$$\begin{cases} \frac{dy_1^{(k+1)}}{dx} = f_1(x, y_1^{(k)}, y_2^{(k)}, y_3^{(k)}, y_4^{(k)}) \\ \frac{dy_2^{(k+1)}}{dx} = f_2(x, y_1^{(k+1)}, y_2^{(k)}, y_3^{(k)}, y_4^{(k)}) \\ \frac{dy_3^{(k+1)}}{dx} = f_3(x, y_1^{(k+1)}, y_2^{(k+1)}, y_3^{(k)}, y_4^{(k)}) \\ \frac{dy_4^{(k+1)}}{dx} = f_4(x, y_1^{(k+1)}, y_2^{(k+1)}, y_3^{(k+1)}, y_4^{(k)}) \end{cases} \quad (43)$$

where $y_i^{(k+1)}$ and $y_i^{(k)}$ are the approximations of the solution y_i at the current and the precedent iteration, respectively (Fig. 2).

At each iteration, the orthogonal collocation on the finite element method is applied to each linear differential equation. Thereafter, we can calculate the uncoupling error by using the following formula:

$$\text{Error} = \text{Max}\Big(\|y_1^{(k+1)} - y_1^{(k)}\|_2, \|y_2^{(k+1)} - y_2^{(k)}\|_2, \|y_3^{(k+1)} - y_3^{(k)}\|_2, \|y_4^{(k+1)} - y_4^{(k)}\|_2\Big) \quad (44)$$

where $\|\cdot\|_2$ is the Euclidean norm.

This procedure gives the solution of the problem, when the error is under a given small epsilon ($\varepsilon \sim$ 1.0e−10).

To explain the procedure, we consider the below differential equation in the domain:

$$y'(x) + a(x)y(x) = f(x) \quad (45)$$

The domain Ω is divided into n elements. After that, the orthogonal collocation is applied in each element $(\Omega^{(i)})_{i=1\ldots n.}$ (Fig. 3(a)).

For the choice of the internal collocation points, we use the roots of the Jacobi orthogonal polynomials of degree N defined in the domain [01].

$$J_N^{(\alpha,\beta)}(x) = \sum_{i=0}^{N} (-1)^{N-i} \gamma_{N,i} x^i \quad (46)$$

where

$$\gamma_{N,i} = \frac{N-i+1}{i} \frac{N-i+\alpha+\beta}{i+\beta} \gamma_{N,i-1} \quad (47)$$

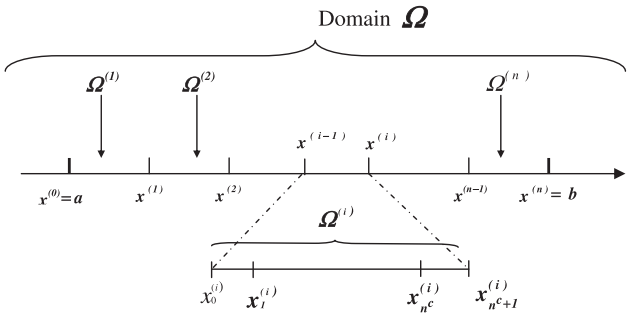

Fig. 2. Finite elements collocation discretizing.

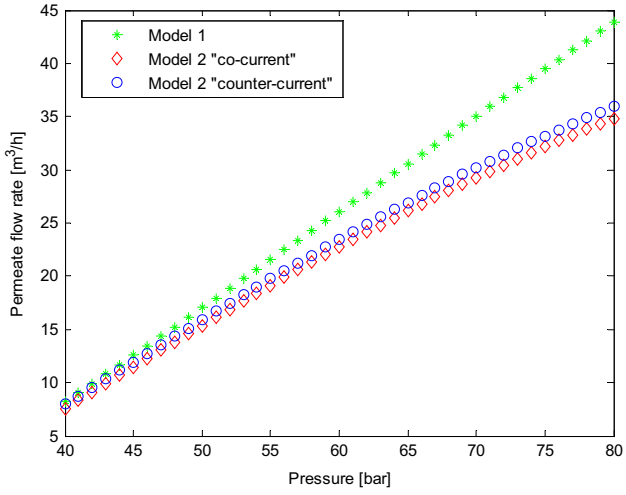

Fig. 3. Permeate flow rate vs. pressure.

with $\gamma_{N,0} = 1$.

α and β are the polynomial characteristic parameters.The elementary solution of Eq. (36) in the ith element is given by:

$$y^{(i)}(x) = \sum_{j=0}^{n^c+1} y_j^{(i)} l_j(x) \quad (48)$$

where n^c is the number of internal collocation points and $l_j(x)$ is the jth degree Lagrange polynomials.Substitution of Eq. (46) into Eq. (45) generates residual $R(x)$:

$$R(x) = \frac{dy^{(i)}(x)}{dx} + a(x)y^{(i)}(x) - f(x) \quad (49)$$

The weighted functions ψ_J are then used to reduce the residual to a minimum value, for $j = 0 \ldots n^c + 1$:

$$\psi_j(x) = \begin{cases} 1 & \text{for } x = x_j^c \\ 0 & \text{for } x \neq x_j^c \end{cases} \quad (50)$$

and

$$\int_{x_o^{(i)}}^{x_{n^c+1}^{(i)}} R(x)\psi_j(x)dx = 0 \quad (51)$$

Consequently:

$$R(x_j^c) = 0 \quad (52)$$

Substituting the expressions of $\frac{dy^{(i)}}{dx}(x_j^c)$ and $y^{(i)}(x_j^c)$ in Eq. (44) leads to a linear system with (n^c+2) equations and (n^c+2) unknowns.

$$M^{(i)} y^{(i)} = b^{(i)} \quad (53)$$

$M^{(i)}$ and $b^{(i)}$ are the elementary matrix and its second member in the ith element $\Omega^{(i)}$By applying the same procedure to each element$(\Omega^{(i)})_{i=1,\ldots,n}$, n systems of algebraic linear equations are obtained. These linear systems are assembled into a global system expressed as follows:

$$M^G y = b^G \tag{54}$$

where M^G and b^G are the global matrix and its second member. The vector y represents the global solution of Eq. (38) on Ω.

4. Model verification and computer simulation

Mathematical models developed above are used to simulate the operation of the reverse osmosis desalination unit of Bousfer in the west of Algeria.

Inaugurated on 18 July 2005, the sea water desalination plant of Bousfer was constructed jointly by the economic public entreprise and the water treatment Spanish company of S.E.T.A "Sociedad Española de Tratamiento de Agua." This plant has a total capacity of 5,000 m^3/d which consists of two lines of production.

The table below summarizes specifications of a line of production (Table 1).

The measured variables used to control the process and technical specifications of the measuring apparatus are described in Table 2.

4.1. Simulation without concentration polarization

By neglecting the concentration polarization phenomenon, we assume that the salt concentration profile in the feed side does not change, and thus, the

Table 1
Technical and membrane specifications of a line of production

Technical specifications	*Membrane specification*		
Production capacity	2,500 m^3/d	Length	1,000 mm
Hourly flow production	104.17 m^3/h	Membrane diameter	200 mm
Hourly flow feed	260 m^3/h	Membrane surface	37.16 m^2
Pressure	69 bars	Nominal rejection	99.80%
Recovery	40%	Minimal rejection	99.70%
Feed water specifications	*Treated water specifications*		
pH	8.1	pH	6.5–7.5
Na^+	12,179 mg/l	Na^+	<175 mg/l
Mg^{++}	1,387 mg/l	Mg^{++}	<30 mg/l
Ca^+	499 mg/l	Ca^+	<10 mg/l
HCO_3^-	158 mg/l	HCO_3^-	<30 mg/l
Cl^-	21,555 mg/l	Cl^-	<250 mg/l
SO_4^-	3,200 mg/l	SO_4^-	<40 mg/l
Total salinity	39,355 mg/l	Total salinity	<39,355 mg/l

Table 2
Technical specifications of measuring apparatus

Measured variables	Instruments	Precision	Range of measurement
Conductivity resistivity total dissolved solid	Conductivity, resistivity, salinity transmitter	±2% of reading value	0.01–400,000 μS/cm 10 kΩ/cm–100 MΩ/cm 0.023–200 000 ppm
Flow rate	Flow transmitter	±0.5% of reading at 25°C thermal sensitivity shift: ±0.005% of reading per °C	Not specified
Pressure	Diaphragm pressure gauge	Accuracy class 1.6 at 20°C thermal sensitivity shift:±0.8%/10 K of full scale value	0–100 bar
pH/ORP "oxidation reduction potential"	pH/ORP transmitter	±0.03 pH ±2 mV ORP	0–14 pH −1,000 to +2000 mV

gradient of the solute concentration can be s expressed as: $\Delta C = C_F - C_P$.

First, a simulation was run without taking into account this phenomenon. The obtained results are summarized in Table 3.

The real parameters are directly read from the measuring devices (flow meter, barometer, and conductivity meter).

Differences with design parameters and real parameter express the relative deviations with simulation values.

The first observation is that the simulation results are closer to the real values than those of design. The results obtained by simulation with the first mathematical model show significant deviations. These differences are more significant compared with the real values.

The second mathematical model gives results better than those of the first model. The deviations are in an acceptable range. They are comprised between 1.51 and 8.89% for the co-current, and between 1.87 and 8.89% the counter-current flow pattern. These differences are small compared with the real values.

The second mathematical model is more adequate to describe the operation of a reverse osmosis module in the absence of the concentration polarization phenomenon. The flow direction has less when this phenomenon is neglected. Indeed, the obtained results with the two flow patterns (co-current and counter-current) are very close.

4.2. Simulation with concentration polarization

A second simulation was run to study the effect of the concentration polarization phenomenon. The results obtained are summarized in Table 4.

The second simulation results are closer to the design and the real parameters than those of the first model, and this for both models.

For the first model, the fact of taking into account the polarization concentration phenomenon reduces the differences between the simulation values and those of the real and the design ones.

The results simulation obtained with the second model with his two variants are closer to the real and design parameters. The deviations are less important.

The general observation is that the fact of taking into consideration the concentration polarization phenomenon allows for more accurate values.

We observe also that the results of simulation with the co-current flow pattern are closer. Indeed, this is the flow pattern used in the sea water desalination plant of Bousfer.

The values obtained by simulation show also the importance of the counter-current flow. According to these results, the permeate flow is more significant: 25.56 m^3/h for the counter-current and 24.79 m^3/h for the co-current. There is a difference of 0.77 m^3/h. This report confirms the results obtained by the study made by Absar et al. [7].

4.3. Study of pressure and flow pattern effects

This study is carried out on both mathematical models. It allows us to follow the changes in principal parameters (permeate and retentate) as a function of pressure.

Fig. 3 shows the permeate flow rate variation with applied pressure. The results obtained with the two models are in agreement with the membrane transport solution-diffusion theory which states that the solvent

Table 3
Comparison between simulations results, design, and real parameters (without concentration polarization)

Developed mathematical models		Permeate		Retentate	
		Flow rate (m^3/h)	Concentration (g/l)	Flow rate (m^3/h)	Concentration (g/l)
Design parameters		26.40	0.45	40.10	64.40
Real parameters		24,80	0,50	41.70	61.89
Model 1	Results	37.40	0.26	29.10	88.79
	Difference with design parameters	41.67%	42.22%	27.43%	37.87%
	Difference with real parameters	50.81%	48.00%	30.22%	43.46%
Model 2 co-current	Results	25.43	0.49	41.07	62.84
	Difference with design parameters	3.67%	8.89%	2.42%	2.42%
	Difference with real parameters	2.54%	2.00%	1.51%	1.53%
Model 2 counter-current	Results	25.65	0.49	40.85	63.18
	Difference with design parameters	2.84%	8.89%	1.87%	1.89%
	Difference with real parameters	3.43%	2.00%	2.04%	2.08%

Table 4
Comparison between simulations results, design, and real parameters (with concentration polarization)

Developed mathematical models		Permeate		Retentate	
		Flow rate (m^3/h)	Concentration (g/l)	Flow rate (m^3/h)	Concentration (g/l)
Design parameters		26.40	0.40	40.10	64.40
Real parameters		24.80	0.50	41.70	61.89
Model 1	Results	28.78	0.41	37.72	68.44
	Difference with design parameters	9.02%	2.50%	5.94%	6.27%
	Difference with real parameters	16.05%	18.00%	9.54%	10.58%
Model 2 co-current	Results	24.79	0.51	41.71	61.89
	Difference with design parameters	6.10%	27.50%	4.01%	3.90%
	Difference with real parameters	0.04%	2.00%	0.02%	0.00%
Model 2 counter-current	Results	25.56	0.50	40.94	63.04
	Difference with design parameters	3.18%	25.00%	2.09%	2.11%
	Difference with real parameters	3.06%	0.00%	1.82%	1.86%

flow rate through the membrane is linearly proportional to the effective pressure difference across the membrane (Eq. (1)) [29]. This linear dependency is well observed in the first model which is a direct application of this theory.

However, for the second model, the increase is gradual at higher pressure. This non-linear behavior is explained by the fact that the solvent flux does not increase without limit and must reach a finite value as the applied pressure becomes very large [30,31]. This non-linearity is a result of salt accumulation at the membrane surface which leads to an increase in the osmotic pressure. The effective driving force is then reduced and also the permeate flux.

In Fig. 4, the permeate concentration is plotted vs. pressure. The obtained results show a decrease in permeates solute concentration with increase in applied pressure. As shown in Eq. (6), the flux of solute through the membrane is proportional to the gradient of the solute concentration and remains fairly constant over the range of the applied pressure [29]. Thus, more solvent passes through the membrane relative to solute, as pressure increases, leading to a decrease in permeate solute concentration. It can be seen that solute concentration, in the case of the first model, is less important as the applied pressure increases. This is due to the rise of solvent flow rate as shown in Fig. 3.

Figs. 5 and 6 show the retentate flow rate and concentration as a function of pressure.

As observed previously, results obtained for both mathematical models are very close. However, a deviation between these values appears at a pressure of 55 bars. It becomes more important for higher pressure values.

The Retentate flow rate and solute concentration are related to the permeate ones by the mass balance

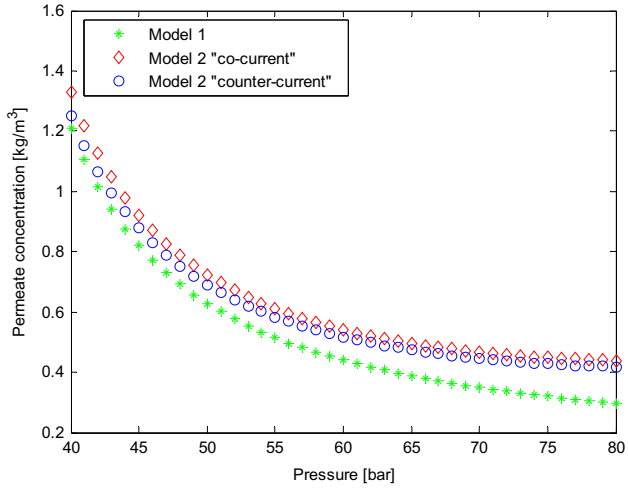

Fig. 4. Permeate concentration vs. pressure.

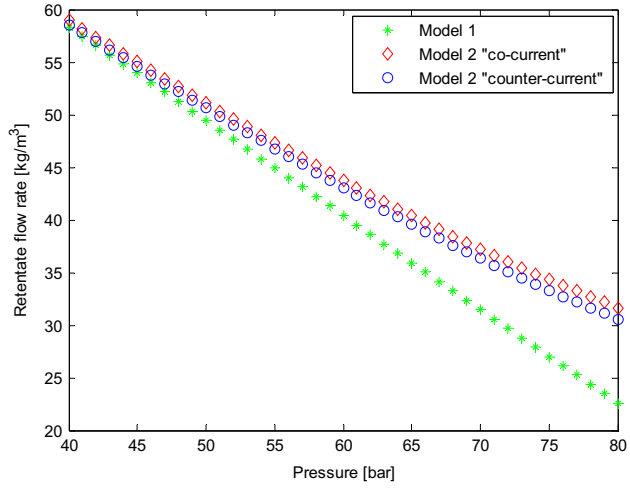

Fig. 5. Retentate flow rate versus pressure.

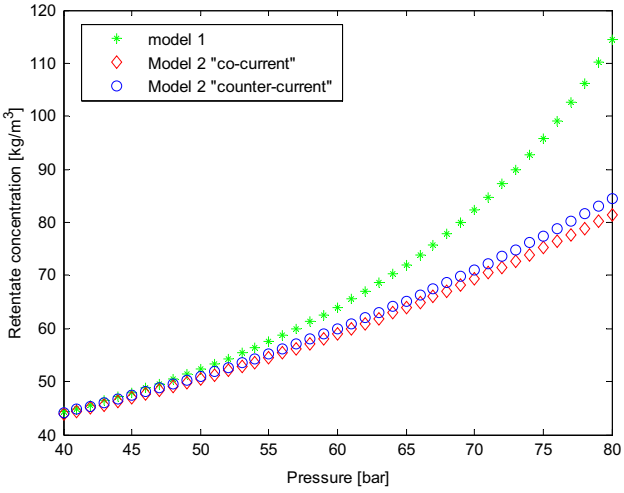

Fig. 6. Retentate concentration versus pressure.

equations. These results are a means to check the accuracy of water and salt mass balance.

5. Conclusion

In this study, two mathematical models are developed to describe the operation of a reverse osmosis desalination unit. These models take into account the concentration polarization phenomenon and propose two modes of circulations: the co-current and the counter-current.

To resolve the split boundary value problem encountered in the second mathematical model, a numerical technique was developed. It consists in combining the advantages of the orthogonal collocation and the finite elements methods. The obtained results are of high precision.

The simulation results obtained from both models are in agreement with the real case of reverse osmosis desalination plant of Bousfer.

Some of the conclusions related with system simulation can be summarized as follows:

- The first mathematical model gives good results only when the concentration polarization phenomenon is taken into account. Otherwise, the results obtained may show significant deviations.
- The second mathematical model with co-current and counter-current mode variants gives good results in both cases, with or without concentration polarization phenomenon.
- The values obtained by simulation show also the importance of the counter-current flow. A permeate quantity of 0.77 m^3/h can be recovered (18.48 m^3 per day).

Symbols

A_w	—	water permeability constant, h/m
B_s	—	solute permeability coefficient, m/h
$b^{(i)}$	—	second member of the elementary matrix in the ith element $rOmega6(i)$
b^G	—	second member of the global matrix
C	—	concentration kg/m^3
D	—	mean diameter, m
D_m	—	mean diameter, m
J_s	—	solute mass flux, kg/m^2
J_w	—	solvent mass flux, kg/m h
J_s	—	Jacobi polynomial of degree N
J_{vw}	—	solvent volumetric flux, m^3/m^2 h
$l_j(x)$	—	Lagrangian interpolation polynomial,
M	—	molar mass, g/mol
$M^{(i)}$	—	elementary matrix in the ith element $\Omega^{(i)}$
M^G	—	global matrix in the domain Ω
n^c	—	number of internal collocation points,
ΔP	—	transmembrane pressure, kg/m h
Q	—	volumetric flow rate, m^3/h
$\dot{Q}$	—	mass flow rate, kg/h
R	—	gas constant, J/mol K
$R(x)$	—	residual
S_a	—	membrane surface, m^2
T	—	temperature, K
t	—	time, h
T_R	—	solution rejection
V	—	volume, m^3
Δx	—	elemental section length, m
$y_i^{(k)}$	—	approximation of the solution y_i at the kth iteration

Greek letters

α	—	polynomial characteristic parameter
β	—	polynomial characteristic parameters
$\kappa\rho_w$	—	proportionality coefficient, m^2/h^2
μ	—	dynamic viscosity, kg/s m
$\Delta\pi$	—	osmotic pressure difference, kg/m h^2
ρ_w	—	water density, kg/m^3

Subscripts

B	—	brine
i	—	inner
F	—	feed side
f	—	fiber side
o	—	outer
P	—	permeate side
p_{avg}	—	product average concentration
R	—	retentate
s	—	shell side
w	—	water

References

[1] J. Marriott, E. Sørensen, I.D.L. Bogle, Detailed mathematical modelling of membrane modules, Comput. Chem. Eng. 25 (2001) 693–700.

[2] A. Idris, A.F. Ismail, S.J. Shilton, R. Roslina, M. Musa, The deduction of fine structural details of reverse osmosis hollow fiber membranes using surface force-pore flow model, Sep. Purif. Technol. 29 (2002) 217–227.

[3] A.S. Kahdim, S. Ismail, A.A. Jassim, Modeling of reverse osmosis systems, Desalination 158 (2003) 323–329.

[4] D.E. Wiley, D.F. Fletcher, Computational fluid dynamics modelling of flow and permeation for pressure-driven membrane processes, Desalination 145 (2002) 183–186.

[5] D.F. Fletcher, D.E. Wiley, A computational fluids dynamics study of buoyancy effects in reverse osmosis, J. Membr. Sci. 245 (2004) 175–181.

[6] M.G. Marcovecchio, P.A. Aguirre, N.J. Scenna, Global optimal design of reverse osmosis networks for seawater desalination: Modeling and algorithm, Desalination 184 (2005) 259–271.

[7] B. Absar, S.E.M.L. Kadi, O. Belhamiti, Reverse osmosis modeling with the orthogonal collocation on finite element method, Desalin. Water Treat. 21 (2010) 23–32.

[8] N.M. Al-Bastaki, A. Abbas, Modeling an industrial reverse osmosis unit, Desalination 126 (1999) 33–39.

[9] N.M. Al-Bastaki, A. Abbas, Predicting the performance of RO membranes, Desalination 132 (2000) 181–187.

[10] N. Al-Bastaki, A. Abbas, Long-term performance of an industrial water desalination plant, Chem. Eng. Process. 43 (2004) 555–558.

[11] S. Senthilmurugan, A. Ahluwalia, S.K. Gupta, Modeling of a spiral-wound module and estimation of model parameters using numerical techniques, Desalination 173 (2005) 269–286.

[12] A. Abbas, Simulation and analysis of an industrial water desalination plant, Chem. Eng. Process. 44 (2005) 999–1004.

[13] T.J. Kennedy, R.L. Merson, B.J. McCoy, Improving flux by pulsed reverse osmosis, Chem. Eng. Sci. 29 (1974) 1927–1931.

[14] J.P. Moulin, M. Rakib, D. Pareau, M. Stambouli, Transfert de matière. Méthodologie [Mass transfer - methodology], Techniques de l'Ingénieur [Engi. Tech.] J1070 (2000) 1-15.

[15] J.P. Moulin, A. Isambert, M. Stambouli, D. Pareau, M. Rajib, Opérations compartimentées idéales [Compartmentalized ideal distillation], Techniques de l'Ingénieur [Eng. Tech.] J1072 (2001) 1-16.

[16] M. Rakib, M. Stambouli, A. Buch, Cinétique du transfert de matière entre deux phases [Mass transfer kinetics between two phases], Techniques de l'Ingénieurs [Eng. Tech.] J1075 (2008) 1-19.

[17] P. Danis, Dessalement d'eau de mer [Sea water desalination], Techniques de l'Ingénieur [Eng. Tech.] J2700 (2003) 1-18.

[18] G. Belfort, Synthetic Membrane Processes, Academic Press, New york, NY, 1984.

[19] R. Darby, Chemical Engineering Fluid Mechanics, Marcel Dekker Incorporation, New York, NY, 2001.

[20] U. Merten, Desalination by Reverse Osmosis, MIT Press, Cambridge, MA, 1966.

[21] L.K. Wong, Y. Hong, N.K. Shammas, Advanced Physicochemical Treatment Processes, vol. 3, Humana Press, New Jersey, NJ, 2004.

[22] R.W. Baker, Membrane Technology and Applications, Second ed., John Wiley, Chichester, 2004.

[23] R.D. Noble, S.A. Stern, Membrane Separation Technology: Principles and Application, Elsevier, Amsterdam, 1999.

[24] P. Nicholls, Introduction: The biology of the water molecule, Cell. Mol. Life Sci. 57 (2000) 987–992.

[25] Mostafa H. Sharqawy, J.H. Lienhard, S.M. Zubair, Thermophysical Properties of Seawater: A Review of Existing Correlations and Data, Desalin. Water Treat. 16 (2010) 354–380.

[26] D.R. Paul, Further comment on the relation between hydraulic permeation and diffusion, J. Polym. Sci. 12 (1974) 1221–1230.

[27] J. Villadson, M.L. Michelson, Solution of Differential Equations Models by Polynomial Approximation, Prentice Hall, New Jersey, NJ, 1978.

[28] S. Tessendorf, R. Gani, M.L. Michelson, Modeling, simulation and optimization of membrane-based gas separation systems, Chem. Eng. Sci. 54 (1999) 943–955.

[29] J. Kucera, Reverse Osmosis: Design, Processes, and Applications for Engineers, Wiley-Scrivener Publishing, Massachusetts, MA, 2010.

[30] D.R. Paul, Reformulation of the solution-diffusion theory of reverse osmosis, J. Membr. Sci. 241 (2004) 371–386.

[31] S. Bhatia, S. DasGupta, S. De, Performance prediction of membrane modules incorporating the effects of suction in the mass transfer coefficient under turbulent flow conditions, Sep. Purif. Technol. 55 (2007) 182–190.